Accumulation Processes of Trace Metals into Arctic Sea Ice: Distribution of Fe, Mn and Cd Associated with Ice Structure

La Kenya Evans[a,b]*, Jun Nishioka[b]

[a]Graduate School of Environmental Earth Science, Hokkaido University, Kita-10, Nishi-5, Kita-ku Sapporo 060-0810, Japan

[b]Institute of Low Temperature Sciences, Hokkaido University, Kita-19, Nishi-8, Kita-ku Sapporo 060-0819, Japan

LKevans@pop.lowtem.hokudai.ac.jp

nishioka@lowtem.hokudai.ac.jp

*Corresponding author e-mail address: LKevans@pop.lowtem.hokudai.ac.jp (L. Evans)

Abstract

Biogeochemical cycling of trace metals in sea ice is important to the productivity of the Arctic Ocean. Unfortunately, the processes by which trace metals accumulate into sea ice are poorly understood. To gain a clearer understanding of the mechanisms behind trace metal accumulation, dissolved (D, <0.2 µm), and labile particulate (LP = Total Dissolvable - Dissolved) iron (Fe), manganese (Mn), and cadmium (Cd) concentrations were compared to the structure observed in sea ice. Samples were pre-concentrated via solid-phase extraction on NOBIAS

Chelate PA-1 resin and analyzed on a Graphite Furnace Atomic Absorption Spectrometer. Using photographic analysis for the percentage of pore microstructure and $\delta^{18}O$ analysis, sea ice structure was determined to be snow ice, granular ice (frazil ice), mixed ice (granular and columnar ice) and columnar ice. Salinity and nutrients were low, indicating brine drainage and multi-year ice. High trace metal concentrations in snow ice indicated meteoric snow was a source of trace metals to sea ice. High concentrations of LPFe in granular ice indicated entrainment of suspended particulate trace metals by frazil ice during the formation of the granular ice structure. Whereas the high concentrations of DFe and DMn in granular ice may have been due to reduction from LPFe and LPMn after particle entrainment, indicating chemical transformation processes. Low dissolved and labile particulate trace metal concentrations in mixed and columnar ice indicated a release due to brine drainage. Our study clearly indicates that the differences observed in trace metals among sea ice structures, showed that sea ice formation, chemical reduction and brine release were the processes driving trace metal accumulation and release in the Arctic sea ice.

Key Words: Sea ice structure; Trace metals; Dissolved; Labile Particulate

Introduction

The Arctic Ocean is characterized by a persistent layer of perennial (multi-year) sea ice during the summer. Multi-year ice is a buffer for solar radiation and a source of both freshwater and trace metals into the Arctic Ocean (Eicken et al., 1995; Tovar-Sanchez et al., 2010). In recent years the Arctic has seen an increase in atmospheric temperatures by 1.6˚C, over double

41 the global average rate for mean temperatures (Overland et al., 2017). During the spring and
42 autumn seasons, the Pacific and Canadian regions have shown the greatest increases in
43 temperature (Przybylak, 2007). Relating this to Arctic sea ice extent, a decreasing trend of -
44 13.2% per decade was observed when compared to the sea ice extent averages of 1981 - 2010
45 (Perovich et al., 2017). In regard to multi-year ice, a decrease of 7 x 10^6 km^2 to 3.5 x 10^6 km^2
46 was observed from 1980 - 2017 (Comiso et al., 2017). Decreases in sea ice extent may point to a
47 regime shift from multi-year ice towards annual (first-year) ice. The presence of thick, multi-
48 year ice dampens wave energy, creating calm waters (Ackley and Sullivan, 1994; Squire and
49 Moore, 1980). The thinner first-year ice is highly influenced by turbulent waves and strong
50 winds. These dynamic conditions can allow for sea ice to collide and thicken through rafting or
51 ridging events (Squire and Moore, 1980; Toyota et al., 2004).

52 Sea ice initially forms when seawater is supercooled (-1.86˚C) creating thermohaline
53 mixing by the convection of heat from the warmer water at depth to the now cooler surface
54 water. With the aid of wind and wave energy frazil ice will form (Eicken, 2003). Frazil ice crystals
55 (3 to 4 mm) form under rough conditions (strong winds or rough currents) at the water's
56 surface, within the water column, or along shelf areas (Kempema et al., 1989; Maykut, 1985;
57 Weeks and Ackley, 1986). As frazil ice float to the surface they create a slush layer that can
58 reduce thermohaline mixing and wind stress (Eicken, 2003; Maykut, 1985). Continual freezing
59 and ice condensing forms grease ice that can solidify up to 10 cm depth (granular ice; Maykut,
60 1985) creating calm conditions under the ice. As seawater congeals downward in calm
61 conditions it forms vertically elongated, prismatic crystal structures known as columnar ice
62 (Eicken et al., 1995; Maykut, 1985). The composition of sea ice is a complex, porous matrix. As

63 sea ice forms, salts concentrate into interstitial dense liquid brine. Some of this brine is released
64 from the ice to ultimately form dense bottom water (Weingartner et al., 1998), while some can
65 be trapped in ice pockets (brine channels) until ice permeability increases (Golden et al., 1998).
66 As brine is retained in sea ice, it can affect the sea ice's nutrient and trace metal composition
67 (Lannuzel et al., 2008; van der Merwe et al., 2011). The rapid decline of multi-year ice in the
68 Arctic may affect the biogeochemical cycling of trace metals, hindering the supply of these
69 metals to the underlying seawater.

70 Within the polar oceans, sea ice is a source of trace metals to the underlying seawaters
71 (Grotti et al., 2005; Sedwick and DiTullio, 1997). The Ross Sea concentrations of particulate
72 (>0.4 μm) and dissolved (<0.4 μm) metals in sea ice were enriched up to two orders of
73 magnitude when compared to the underlying seawater (Grotti et al., 2005). As sea ice melts, it
74 can supply trace metals to the underlying surface seawaters. Aguilar-Islas et al. (2008) found
75 that melting sea ice in the outer Bering Sea shelf provided additional DFe to ice-edge
76 phytoplankton that may have increased their biomass and utilization of available nitrate. A
77 study done by Evans and Nishioka (2018) observed drift sea ice from the Chukchi Sea was
78 dominated by the labile particulate (LP = difference between the total dissolvable; TD,
79 unfiltered sample; and dissolved; D, <0.22 μm filtered sample) fraction of iron (Fe), manganese
80 (Mn) and cadmium (Cd) when compared to Chukchi surface seawater. It is possible that the
81 consistent flushing of seawater, or brine drainage released the available dissolved metals in the
82 drift sea ice. The migration of sea ice in the Arctic Ocean allows sea ice to transport
83 incorporated materials (such as trace metals, nutrients and sediments) from areas of formation
84 (e.g. shelf seas) to areas of melting (e.g. open ocean, basins; Darby, 2003; Eicken et al., 2005).

85 This gives sea ice the potential to circulate trace metals biogeochemically, increasing its
86 importance as a source in the Arctic Ocean (Grotti et al., 2005; Lannuzel et al., 2008). To add to
87 the body of knowledge for the biogeochemistry of trace metals in polar sea ice, the goal of this
88 study was to observe the mechanisms behind accumulation and release of trace metals from
89 Arctic sea ice.

90 Observations of ice structure can allow for the detection of the formation process of sea
91 ice. It is possible that, as sea ice forms, it may incorporate trace metals into the ice. Trace
92 metals may also accumulate into ice after it is established. The processes by which trace metals
93 are retained or released from the ice are varied and not clear. In seawater, Fe, Mn and Cd
94 exhibit different chemical sensitivity and behavioral (i.e. oxidation-reduction reactions)
95 properties. Manganese displays a scavenging-type distribution where it has interactions with
96 particles and shelf sediments. Cadmium is an example of a nutrient-type distribution. This metal
97 is influenced by biological processes (i.e. phosphate cycle) and organic particulate matter. Iron
98 shows more of a scavenging-type distribution and can also display nutrient-type behavior
99 (Bruland et al., 1994; Bruland and Lohan, 2006). Comparisons of Fe and Mn yield different
100 reduction potentials (Landing and Bruland, 1987; Saager et al., 1989) which may influence the
101 concentrations of their size fractions (Evans and Nishioka, 2018). Relating the concentrations of
102 trace metals that display different actions in sea ice structure, from an Arctic core sample, may
103 aid in revealing mechanisms behind trace metal accumulation.

104 *Materials and Methods*

105 *Materials Cleaning Procedure*

High-density polyethylene (HDPE) jars, HDPE buckets, and low-density polyethylene (LDPE) bottles (HDPE, LDPE, Nalgene Company, Limited), Teflon (bottles and tubbing), filters (0.22 µm, Durapore, Millipore Ltd.), and other plastics were cleaned using the methods outlined in previous studies (Nishioka et al., 2001; Takeda and Obata, 1995) for trace metal clean sampling and analysis of sea ice. Ceramic knifes used during the cleaning (planing) step for sea ice were cleaned in an onshore clean room by the following procedure: knives were placed in 5% Extran® (alkaline and phosphate-free liquid, Merck) for one day, rinsed with reverse osmosis (RO) water then placed in ultrapure hydrochloric acid (0.1 M HCl, Tamapure-AA-10, Tama Chemical Ltd.) for one day. The knives were rinsed with Milli-Q water (Millipore Ltd.) and air dried on a laminar flow clean bench before use.

An acrylic ice holder (Fig. 1) was used in the ice planing step to keep the ice core sample stable during planing. The ice holder was cleaned by a 5 % Extran® bath for one day, rinsed with RO water and air dried. Ice samples were prepared by planing in a 137 L freezer (cold tub, Panasonic; Fig. 1) located in a dust free clean room. The cold tub was covered with clean plastic, allowing it to maintain the preset temperature (-20˚C). 24 hrs before ice planing, the cold tub was turned on and all planing materials (ceramic knifes, gloves, collection buckets, etc.) were double bagged and placed in the cold tub as the tub cooled down to -20˚C. For each subsequent sample that was planed, the cold tub was cleaned of previous ice waste generated during planing and air dried in the clean room.

Sea Ice Sampling

Sea ice was collected from the Beaufort Sea on August 2013 at ice station 76˚56'N, 138˚38'W during the JIOS cruise aboard the *CCGS Louis S. St-Laurent* (Fig. 2). Sea ice was sampled with a 9 cm diameter corer and the core length was immediately measured with a tape measure (Fig. 3a). The core sample was then cut in half (50 cm and 53 cm respectively), individually placed in coolers and transported to an onboard cold room (-15˚C) before being transported to an onshore cold room (-15˚C). The sample was held for 4 years before analysis.

Milli-Q Ice Contamination Test

The corer used to collect the sea ice was made of metal. Unfortunately, this process can contaminate the outer layers of the sea ice sample for trace metal analysis. To account for this contamination, sea ice is usually cleaned through planing a couple of centimeters off the outer ice layers with acid cleaned ceramic knives. The cleaned inner core of the ice is then analyzed for trace metals. To determine the amount of contamination contributed by ice planing materials (ceramic knifes, plastics and collection buckets), the coring process and the planing procedure, a contamination test was performed on Milli-Q ice. All samples were handled with clean plastic gloves and plastic wrap. In an onshore class 100 clean room, two Milli-Q ice samples were prepared by freezing Milli-Q water in acid cleaned 500 mL HDPE bottles (tops cut off). The resulting ice formed as a cylinder (Milli-Q ice). One day before planing, one of the Milli-Q ice samples was removed from the 500 mL bottle and wrapped in aluminum foil (Foil ice). It was placed in the cold tub to mimic contamination resulting from the coring process during sample collection. The other Milli-Q ice was left untouched in the freezer before the planing step (Milli-Q Clean ice). Each Milli-Q ice was planed separately.

Before ice planing, the ice holder was wrapped in clean plastic and placed in the cold tub (-20˚C). For the Foil ice, the aluminum foil was removed before planing. For the Milli-Q Clean ice, the ice sample was removed from the bottle and immediately planed to minimize handling. For each ice sample two layers (1 cm each) was planed using acid cleaned ceramic knifes. A new, clean knife was used to plane each side as evenly as possible. All ice pieces that were in contact with the planing materials were collected into acid cleaned 325 mL HDPE jars. The planed ice core was collected in acid cleaned HDPE buckets and all samples were melted at room temperature in a dust free clean room. Melted samples were immediately acidified by ultrapure HCl (final concentration 0.05 M with <pH 2.0, Tamapure-AA-10) and pre-concentrated via NOBIAS Chelate PA-1 resin (NOBIAS, 150 mg, Hitachi High-Technologies Co.) before analysis on a graphite furnace atomic adsorption spectrophotometer (GFAAS, Hitachi High-Technologies Co.). The Milli-Q ice contamination test results are shown in Figure 4 (pre-concentration factor ranging from 4.6 - 8.7 times, avg. 7.5 times). Planing 2 cm of ice off the outer core sample was sufficient for trace metal analysis as the ice planing materials and procedure did not contribute contamination to the ice sample.

Sea Ice Planing and Preparation

When the sea ice core sample was planed, a blank sample (Milli-Q water) was frozen (Milli-Q blank) in a 325 mL LDPE jar and set in the cold tub. The Milli-Q blank was used to check that the planing conditions were clear of contamination. The planing of sea ice followed the methods outlined above. Once 2 cm of the outer ice core was planed, the sample was visually observed and separated based on sea ice structure. Pictures of each section were taken with a digital camera to aid with the sea ice structure determination. Pictures were transformed to

black and white and overlaid with a filter to detect the outline of the pore microstructure captured in the pictures (GNU Image Manipulation Program, GIMP). The % white area in the transformed pictures, the area that represents the outline of the pore microstructure (hereafter porosity %), was calculated using R analysis package (R Core Team 2013; Ooms, 2018; Mouselimis, 2018). This analysis allowed for an objective discrimination between granular and columnar ice, and the identification of mixed (granular plus columnar) ice. All planed samples, and the Milli-Q blank, were placed in acid clean HDPE buckets and melted at room temperature in a clean room.

Immediately after melting, samples were separated for trace metal analysis, salinity, $\delta^{18}O$, and nutrients. Nutrient samples were re-frozen immediately after melting and stored before analysis. To prepare for trace metal analysis, a portion of the meltwater was separated into acid cleaned 125 mL LDPE bottles for total dissolvable samples and immediately acidified with ultrapure HCl (final concentration 0.05 M with <pH 2.0, Tamapure-AA-10). Another portion of meltwater (dissolved) was immediately filtered by 0.22 µm Durapore filters (Milipore) with a peristaltic pump (Cole-Parmer Instrument Company), Teflon micro-tubing and a Teflon filter holder into acid cleaned 125 mL LDPE bottles. The filtrate was immediately acidified with ultrapure HCl (final concentration 0.05 M with <pH 2.0, Tamapure-AA-10). All samples were held for 3 weeks in a clean room before analysis.

Analytical Methods

NOBIAS Pre-Concentration Method

189 Chemicals used during the pre-concentration process held a chemical grade of reagent,
190 pure or ultrapure and were prepared with Milli-Q water. The NOBIAS Chelate PA-1 chelating
191 resin has a high affinity for trace metals and the ability to separate alkali- and alkaline-earth
192 metals from sea ice and seawater (Evans and Nishioka, 2018; Minami et al., 2015; Sohrin and
193 Bruland, 2011). The cleaning, setup and methods for the NOBIAS pre-concentration are detailed
194 in Evans and Nishioka (2018). Briefly, a 3.36 M acetic acid-ammonium acetate (HAcO-NH_4AcO)
195 buffer was made from glacial acetic acid (Optima, Fisher Chemical), 20% NH_4OH (ultrapure,
196 Tamapure-AA-10) and Milli-Q water. A portion of this buffer was diluted to 0.05 M HAcO-
197 NH_4AcO and purified twice via NOBIAS before use.

198 Pre-concentration for both total dissolvable and dissolved sea ice and ice blank samples
199 with the NOBIAS resin were modified from the methods detailed in Evans and Nishioka (2018).
200 The resin column was initially cleaned by loading 1 M ultrapure HNO_3 (Tamapure-AA-100, Tama
201 Chemical Ltd.) at 1 mL/min. and then conditioned with Milli-Q water and 0.05 M HAcO-NH_4AcO
202 (both at 3 mL/min.). During the conditioning step, 1.8 mL of 3.6 M HAcO-NH_4AcO was added to
203 30 mL of sample. The sample's pH was adjusted to pH 6 ± 0.1 with 20% NH_4OH then loaded
204 onto the resin column (3 mL/min.). The 0.05 M HAcO-NH_4AcO (3 mL/min.) buffer followed the
205 sample to flush out any interferences (i.e. salts) and the column was disconnected from the
206 manifold. The eluent was back-eluted by an acid cleaned hand syringe with 10 mL of 1 M
207 ultrapure HNO_3 into an acid clean polyethylene collection tube. To calculate the original trace
208 metal concentration in the meltwater, both the initial and final weights of the eluent and
209 sample bottles were determined. If multiple samples were pre-concentrated, the procedure
210 would begin at the initial cleaning step (1 M HNO_3 at 1 mL/min.).

All pre-concentrated samples were analyzed on a GFAAS. Single element standards were made from diluting 1000 ppm individual standards (Wako Chemical Ltd.) of Fe, Mn and Cd in 1 M ultrapure HNO_3. The pre-concentration detection limit (DL) was calculated with pre-concentrated Milli-Q procedural blanks by multiplying their standard deviation by three (n = 6). For each metal the detection limit yielded: 2.0 nM Fe, 0.4 nM Mn and 0.05 nM Cd. After pre-concentration and analysis with GFAAS, ice core sample data was compared to the pre-concentrated DL. Comparison with the pre-concentrated DL allowed for accurate detection of the lowest concentrations of elements (Fe, Mn or Cd) within a sample. Pre-concentrated ice core sample data that was above the DL was calculated with the concentration factor (range 2.3 - 3.0 times) and presented within this study. Validation of the NOBIAS pre-concentration method was done with NASS-6 reference seawater materials (National Research Council of Canada). Measured values (n = 8) showed 9.5 ± 1.3 nM Fe, 11.2 ± 1.4 nM Mn and 0.3 ± 0.1 nM Cd that was similar to the National Council of Canada's certified values (8.9 ± 0.8 nM Fe, 9.6 ± 0.9 nM Mn, and 0.3 ± 0.02 nM Cd).

Analysis of Salinity, $\delta^{18}O$, and Nutrients

For salinity measurements, a portion of the sea ice meltwater was measured for chloride ions using a chloride analyzer (Model SAT-500, Towa Electronic Industry, repeatability: <0.5%). A lab standard regression curve (paired salinity and chloride; AUTOSAL 8400B salinometer, Ocean Scientific International Ltd.) was used to determine the salinity of the meltwater from the measured chloride values. Oxygen isotopes for sea ice were determined by an isotope water analyzer (Picarro, Inc.) with an analytical precision of ± 0.3%. For the nutrient analysis a portion of sea ice meltwater that was frozen was re-melted at room temperature in

233 an onshore class 100 clean room. Samples were analyzed on a continuous flow system
234 autoanalyzer (QuAArto, BL TEC, Inc.). Standard solutions were made in Milli-Q water to match
235 the low salinity of the sea ice samples.

236 *Results*

237 *Physical and Chemical Properties in Sea Ice*

238 Immediately after the ice sample was collected, the sea ice core length was measured to
239 103 cm and photographed (Fig. 3a). The sea ice structure was determined by visual inspection
240 using the terms defined by Petrich and Eicken (2010). Usually thick (5 mm) and thin (0.5 mm)
241 ice sections illuminated by polarized light are used to observe the crystallographic structure
242 (textural variability, boundary layers, etc; Toyota et al., 2004) of sea ice. These sections are cut
243 with a metal saw, contaminating the ice samples for trace metal analysis. To avoid adding
244 contamination during the ice structure analysis, visual observations, photographic image
245 analysis and porosity % analysis were performed on planed ice samples in this study.

246 The ice structures of the planed ice core were analyzed in six sections: 0 - 24 cm, 24 - 41
247 cm, 41 - 58 cm, 58 - 75 cm, 75 - 91 cm and 91 - 103 cm (Fig. 3b). Each section was homogenized
248 before separation for salinity, $\delta^{18}O$, nutrients and trace metal analysis. Sections were large to
249 account for the volume necessary for the NOBIAS pre-concentration before trace metal
250 analysis. The 0 - 24 cm section showed snow/slush-like ice that was in the transition of turning
251 more solid. The porosity % (Fig. 3c) of this section show 1.9, indicating highly porous ice. A
252 piece of solid ice (below 9 cm; Fig. 3b) may represent snow that was melted and re-frozen,
253 hinting at multi-year ice. Sections 24 - 75 cm showed ice with disconnected pore microstructure

254 that was more apparent than in the 0 - 24 cm section. The porosity % for each section (0.7%,
255 1.3%, and 0.6%, respectively, Fig. 3c) were lower than seen from 0 - 24 cm. From 75 - 91 cm the
256 porosity % (0.5) was similar to the 58 - 75 cm section, but it lacked obvious pore microstructure.
257 Instead the structure represented solid ice intermixed with ice that had disconnected pore
258 microstructures. From 91 - 103 cm solid ice (porosity 0.04%) was observed.

259 Sea ice salinity was observed to be low (1.3 to 2.1, Fig. 5a). In first-year ice, typical
260 salinity profiles exhibit a C-type profile (Cox and Weeks, 1988) with salinities around 5 - 15
261 (Eicken et al., 1995). As sea ice ages and thickens, desalination processes decrease the salinity
262 to below 4 characterizing multi-year ice (Cox and Weeks, 1974; Eicken et al., 1995). Therefore,
263 the observed salinity for this study indicates multi-year ice. It is possible that brine may have
264 been artificially released during the coring process, lowering salinity, nutrient and trace metal
265 concentrations within the ice core sample. After coring an adjacent ice core was tested for
266 salinity. High salinity values would indicate that brine was present in the adjacent sea ice core
267 after coring. If brine was released in the sea ice, before coring, salinity values would be low in
268 the adjacent ice core. The concentrations from the adjacent ice core matched the
269 concentrations within the ice core sample after a 3 year holding period. Therefore, the brine
270 was released from the sea ice sampling site before coring. Nutrient concentrations in the ice
271 core were below the DL (0.02 µmol/L NO_3 + NO_2, 0.02 µmol/L PO_4, and 0.1 µmol/L SiO_2). It is
272 possible that the nutrients, along with the salinity, were released from the sea ice during
273 desalination before coring. Measured $\delta^{18}O$ values are shown in figure 5b and were used to
274 identify source water to sea ice. As seawater freezes to form sea ice, it induces the
275 fractionation of oxygen isotopes (Toyota et al., 2004; Ukita et al., 2000). This allows for the

276 comparison of $\delta^{18}O$ with sea ice to determine the water source (freshwater or seawater).
277 During the JIOS cruise, an average surface seawater (<50 m) $\delta^{18}O$ value for the area near the
278 sampling site was observed at -3.38‰ (Yamamoto-Kawai personal comm.). It is possible that
279 sea ice melt, Pacific origin water and river water mixed with the surface seawater, to decrease
280 the $\delta^{18}O$ value (Yamamoto-Kawai et al., 2008). A freshwater sample was collected from snow-
281 like ice observed on the surface of the ice sample. The $\delta^{18}O$ was observed to be -4.1‰ (Surface;
282 Fig. 5b), indicating a meteoric snow source. Although there was a strong freshwater influence
283 on the seawater in this study, the seawater $\delta^{18}O$ values was higher than that for the surface
284 snow value allowing for the distinction between freshwater and seawater sources during sea
285 ice formation. The sea ice section from 0 - 24 cm had a $\delta^{18}O$ value of -2.6‰. This section may
286 represent a mixture of both freshwater and seawater sources. Sea ice sections from 24 - 103 cm
287 had $\delta^{18}O$ values ranging from -1.2 to -0.8‰. This indicates that these sections were sourced
288 from seawater (see discussion). The ice structure was then determined by comparing the $\delta^{18}O$
289 values with the picture analysis and porosity % analysis from each section. Snow ice was
290 dominate for section 0 - 24 cm, granular ice for section 24 - 75 cm, mixed ice for section 75 - 91
291 cm and columnar ice for section 91 - 103 cm. The ice structures determined from these
292 analyses will be used for the remainder of this study.

293 *Trace Metals*

294 *Dissolved Metals in Sea Ice*

295 Sea ice concentrations for DFe ranged from 1.1 to 4.8 nM (Fig. 6a). Snow ice (3.1 nM)
296 and granular ice (3.6 ± 0.8 nM, n = 3) showed higher concentrations when compared to mixed

297 ice (1.1 nM) and columnar ice (1.3 nM). Dissolved Mn in sea ice ranged from 1.4 to 11.0 nM
298 (Fig. 6c). The snow and granular ice showed higher concentrations (5.5 nM and 8.5 ± 3.5 nM,
299 respectively) than mixed (1.5 nM) and columnar (1.4 nM) ice. Dissolved Cd in sea ice was low
300 and ranged from <DL to 0.2 nM (Fig. 6e). Dissolved Cd was only observed in snow (0.1 nM) and
301 granular (0.1 ± 0.06 nM) ice. Within this sea ice sample the snow and granular ice structures
302 held the highest trace metal concentrations.

303 *Labile Particulate Metals in Sea Ice*

304 Concentrations of labile particulate metals seemed to be dependent on the trace metal.
305 LPFe in sea ice ranged from 2.2 to 475.6 nM (Fig. 6b). The snow (92.3 nM) and granular (232.9 ±
306 172 nM, n = 3) ice had higher LPFe concentrations when compared to the mixed (7.6 nM) and
307 columnar (2.2 nM) ice. Labile particulate Mn was low in sea ice and ranged from <DL to 0.5 nM
308 (Fig. 6d). Labile particulate Mn was detected in snow (0.5 nM), granular (0.1 nM) and mixed
309 (0.08 nM) ice. Labile particulate Cd was also low in sea ice ranging from <DL to 0.08 nM (Fig. 6f)
310 and only detected in granular ice (0.03 ± 0.03 nM, n = 3). The LP fraction for trace metals were
311 high in the snow and granular ice structures as observed with the D fraction. For both fractions,
312 concentrations of trace metals were dependent on the metal.

313 *Discussion*

314 *Sea Ice Stratigraphy and Formation Processes*

315 Sea ice formation processes are reflected in the ice structures that are created and
316 manifested in distinct vertical sections of an ice core. In the snow ice section, the observed $\delta^{18}O$
317 showed a mixture of freshwater (meteoric snow) and seawater (Fig. 5b). Snow ice formation

318 may have occurred through a flood-freeze cycle (Ackley et al., 1990). Generally meteoric snow
319 will collect and accumulate onto the surface of sea ice. As more snow is added, the weight can
320 compress sea ice below the water's surface. Snow ice can then form as accumulated meteoric
321 snow mixes with incoming seawater (Fritsen et al., 1998; Hudier et al., 1995). At the bottom
322 part of the snow ice section, slush-like ice was observed (Fig. 3b, above 24 cm). Slush ice is
323 created by seawater mixing with snow, further indicating that the flood-freeze cycle process
324 may have occurred.

325 A large portion of the sea ice sample was composed of granular ice (Fig. 3c). Granular ice
326 has two genetic classifications: snow-granular and frazil-granular that can be identified through
327 grain (via thick, 5 mm, or thin, 0.5 mm, sections) and $\delta^{18}O$ analysis (Toyota et al., 2004; Ukita et
328 al., 2000). Since it was not possible to make trace metal clean thick or thin sections for grain
329 analysis to classify ice stratigraphy, $\delta^{18}O$ was used to differentiate between the two genetic
330 classifications. Frazil-granular ice usually has higher $\delta^{18}O$ values (seawater) than observed for
331 snow-granular ice (freshwater). The $\delta^{18}O$ in granular ice for this study yielded high values (-0.8
332 to -1.1‰) due to isotopic fractionation from a seawater source (Fig. 5b; Lange et al., 1990;
333 Toyota et al., 2004; Ukita et al., 2000). Therefore, the granular ice section was composed of
334 frazil ice. The mixed ice section (75 - 91 cm) yielded similar porosity % (0.5) values as observed
335 in the granular ice. The photo analysis of the thick section indicated that this structure was not
336 fully granular ice but a mixture of granular and columnar ice (Fig. 3b,c). Mixed ice may be an
337 indication, along with frazil ice, of dynamic growth processes (Toyota et al., 2007). Mixed ice
338 can form during rough currents and high winds which can allow for: 1) the formation of new
339 frazil ice over established/deformed ice regardless of ice texture, 2) the overlapping of ice

sheets, and 3) frazil ice formation in between floe gaps caused by rafting/ridging event (Hopkins et al., 1999; Lange and Eicken, 1991; Lange et al., 1989). The observed columnar ice within this sample was created through the congelation of seawater in calm conditions (Toyota et al., 2004). This is supported by observations of the ice structure from photo analysis (Fig. 3b), and low porosity % value (Fig. 3c). It should be noted that sea ice within a single ice floe is heterogeneous allowing for the ice stratigraphy within a floe to be variable. The heterogeneity of sea ice may be due to different wind conditions during ice growth (Eicken and Lange, 1989). Therefore, the use of one ice core sample represents only a subset of the trace metal accumulation and release mechanisms that may affect the composition of Arctic sea ice.

Source and Accumulation Processes of Trace Metals into Sea Ice

Ice structure explains the formation processes utilized by sea ice. Comparing ice structure to trace metal concentrations within a single core sample allows the determination of trace metal sources. In addition, the determination of possible mechanisms behind trace metal accumulation in, and release from, sea ice become clearer. In this study the snow ice showed high concentrations of dissolved for all metals and high concentrations of labile particulate for Fe and Mn (Fig. 6). This indicates that one mechanism for trace metal accumulation into sea ice may be snow ice formation through the flood-freeze cycle (Ackley et al., 1990).

Polar snow is mostly composed of water (99.99%), with less than 1% composed of particulate dust and sea salt aerosols (Barrie, 1986; Planchon et al., 2004). The amount of contaminates within Arctic snow can fluctuate depending on anthropogenic activities from Eurasia and North America, with higher particulate dust available in winter than in summer

(Krachler et al., 2005). Trace metals, bound to particulate dust, are then deposited onto sea ice during snow fall. As snow ice forms, these trace metals can become trapped within the ice crystals. Increases in Arctic temperatures have increased water vapor which, along with increased anthropogenic emission, has yielded higher precipitation in the Arctic Ocean (Tovar-Sanchez et al., 2010). Therefore, the high concentrations of LPFe observed in this study may be due to meteoric snow. Lannuzel et al. (2007) observed TDFe and DFe in snow ice from the Antarctic region, indicating that atmospheric deposition was a minor source of trace metals to the snow ice fraction of sea ice when compared to seawater influences. The range of DFe (3.1 nM, Fig. 6a) from snow ice in this study was comparable to that of Antarctic snow (1.0 - 6.5 nM). Total dissolvable Fe from snow ice in this study (92.3 nM Fig. 6b) was observed to be higher than in Antarctic snow (1.8 - 23.7 nM). This indicates that atmospheric deposition may be a source of trace metals to Arctic sea ice. Snow ice from the sub-polar marginal Sea of Okhotsk was also observed as comparable concentrations of DFe (3.7 ± 1.3 nM DFe) with that of snow ice from this study. Although the comparison for the different size fraction of Fe concentrations were variable depending on location, the trace metal trend further supports meteoric snow as a source of trace metals to snow ice. Another possible mechanism for trace metal accumulation from meteoric snow may be the influence of snow meltwater during snow ice formation (Granskog and Kaartokallio, 2004; Marsay et al. 2018). In the current study, results from the $\delta^{18}O$ analysis yielded the snow ice section source water as a mixture of both freshwater and seawater (Fig. 5b). Although the percent contribution from the two water sources was not quantified; it is possible that meteoric snow was a source of trace metals to snow ice.

383 The concentration of trace metals was higher in granular ice than observed in snow ice,
384 indicating another mechanism for trace metal accumulation into Arctic sea ice. As discussed
385 above, the granular ice structure was composed of frazil ice indicating that the high
386 concentrations of LPFe (Fig. 6b) may be explained by particle entrainment. In the Arctic Ocean,
387 frazil ice can form in shallow (<50 m) shelf areas (Dethleff et al., 1998; Eicken et al., 2005;
388 Reimnitz et al., 1994). Turbulence in the water column, due to fall storms, can re-suspend shelf
389 sediments and smaller particles in the water column. Frazil ice can interlock with these
390 suspended particles through suspension freezing and rise together to the water surface
391 (Campbell and Collin, 1958; Nürnberg et al., 1994; Osterkamp and Gosink, 1984; Reimnitz et al.,
392 1992). As frazil ice thickens (from slush ice to floe ice), particles are entrained into the granular
393 ice structure (Dethleff, 2005). Ito et al. (2017) used Acoustic Doppler Current Profiler
394 backscatter data to observe the entrainment of sediments by frazil ice. They found that at a
395 wind speed of 15 - 19 m s^{-1} and a current speed of 1.0 - 1.5 m s^{-1} sediments were re-suspended
396 into the water column where they interlocked with the frazil ice. Through this process, trace
397 metal bound sediments and smaller particles are also scavenged by frazil ice and finally
398 entrained into granular ice (Hölemann et al., 1997; Ito et al., 2017; Lannuzel et al., 2010, 2017),
399 increasing the concentrations of sediment/particle associated metals in the sea ice. Lannuzel et
400 al. (2007) reported that the Fe concentrations in sea ice, made from seawater, were also due to
401 sediment entrainment. Sea ice formed in the southeastern Chukchi and western Beaufort shelf
402 areas is characteristically sediment-laden (Eicken et al., 2005). This sea ice can follow the
403 Beaufort Gyre moving westward further into the Arctic Ocean. Sea ice collected for this study
404 may have formed in the shelf areas of the Beaufort Sea. As the sea ice aged and travelled

following the Beaufort Gyre flow, trace metals may have been added during ridging events or frazil formation in the leads between floes (Lange et al., 1989; Lange and Eicken, 1991; Toyota et al., 2004). Based on the visual observations of sea ice melt in the lab, sediments were not detected in this sample. Labile particulate Fe showed a trend of higher concentrations in granular ice (232.9 ± 172 nM) when compared to mixed and columnar ice (7.6 nM and 2.2 nM respectively; Fig. 6). Particulates derived from fine-grained sediment or organic matter origins (Dethleff, 2005; Kempema et al., 1989; Nürnberg et al., 1994) maybe influential to trace metals. Comparing the trace metal concentrations from snow ice to granular ice yields higher concentrations in the granular ice (with the exception of LPMn; Fig. 6). In addition, the sea ice sourced from seawater in the current study's ice sample yielded more volume than observed for the snow sourced ice. It is possible that a sediment source from a seawater medium is more influential than from atmospheric deposition (Granskog and Kaartokallio, 2004). Thus, particle scavenging during the dynamic growth processes used to form frazil ice allowed trace metals to entrain and accumulate into the granular structure of sea ice.

The process of trace metal accumulation by particle entrainment is further supported by the concentrations of dissolved and labile particulate Cd observed in granular ice (Fig. 6e,f). Cadmium is associated with clay materials (Pardue et al., 1992) and with Fe/Mn oxides in oxic sediments (Guo et al., 1997). As sediments entrain into sea ice, fine silts or clays are effectively retained in the ice crystals (Nürnberg et al., 1994). It is possible that the observed concentrations of Cd in granular ice further indicates the presence of fine particles, possibly sourced from sediments, in this ice structure. Dissolved and labile particulate metal concentrations in granular ice were also observed to be vertically heterogeneous (Fig. 6). The

dynamic environment where frazil ice forms and its non-uniformity (such as shelf seas), have yielded patchy sediment-laden ice within Arctic sea ice (Eicken et al., 2005; Garrison et al., 1983). Patchy entrainment of sediments into sea ice can then translate to heterogeneous concentrations of trace metals observed in sea ice (Evans and Nishioka, 2018). Based on the observations from this and previous studies (Campbell and Collin, 1958; Dethleff, 2005; Hölemann et al., 1997; Ito et al., 2017; Lannuzel et al., 2007, 2010, 2017; Nürnberg et al., 1994; Reimnitz et al., 1992), the accumulation of trace metals into granular ice may be due to frazil ice formation and particle entrainment.

Release Processes of Trace Metals from Sea Ice

Mixed and columnar ice structures in Arctic sea ice yielded trace metal concentrations that were low or below the detection limit (Fig. 6). This indicates a trace metal release mechanism resulting from brine drainage. In the early stages of sea ice formation during fall, most of the seawater salts are released from the ice crystal lattice. In sea ice around 0.05 m thickness, bulk salinity is about 25. As sea ice thickens (1.5 m) the percent bulk salinity can decrease to 5 (Kovacs, 1996). The interstitial salts remaining in the sea ice will concentrate into liquid brine (Kingery and Goodnow, 1963; Untersteiner, 1968). Brine drainage occurs when dense brine convects through permeable ice from cold (top of the ice) to warm (bottom of the ice; Jardon et al., 2013) temperatures. As the ice strives for thermodynamic equilibrium, the movement of brine widens brine channels (Petrich and Eicken, 2010) through the ice lattice increasing the potential for fluid percolation. Relating the ability of brine drainage with sea ice structure, the columnar structure maybe more efficient in releasing brine when compared to the granular structure (Lannuzel et al., 2007). Columnar ice structure can form more slowly

(approximately factor of 2) than granular ice structure (Eicken and Lange, 1989; Weeks and Ackley, 1986). The formation of different ice structures dictates the orientation of brine channels (Spindler, 1994; Weissenberger et al., 1992). In granular ice the branching of brine channels retains the liquid brine until they widen. In the columnar ice structure brine channels have a laminar orientation (Petrich and Eicken, 2010). This can allow brine to be rejected more efficiently (Janssens et al., 2016; Weissenberger and Grossmann, 1998). In sea ice, nutrients have a decreasing linear trend with bulk salinity (Thomas et al., 2010). Therefore, the presence of brine can be detected by its salinity and nutrient concentrations. In this study, the nutrient concentrations analyzed in sea ice were below the detection limit. This indicates that brine, along with the trace metals, was released from the sea ice. Brine has been shown to retain high concentrations of trace metals. In the Antarctic region, concentrations of TDFe and DFe from brine sack-holes were two orders of magnitude higher than the surrounding seawater (Lannuzel et al., 2007). When compared to sea ice, brine concentrations of DFe were elevated (van der Merwe et al., 2011). Dissolved trace metals in brine can thus be influenced by brine release, decreasing their concentrations within sea ice (Lannuzel et al., 2007; van der Merwe et al., 2011). In contrast, PFe concentrations in Antarctic brine have been observed to be low. This indicates that PFe may bind to the brine channel walls or organic matter (Lannuzel et al., 2010). A robust community of phytoplankton and bacteria has been observed in the brine channels of the sea ice interior (Ackley et al., 1979; Horner et al., 1992) and at the sea ice-seawater interface (Spindler, 1994). Ice algae and bacteria create exopolymeric (i.e. exopolysaccharides) gel like substances. They are composed of uronic acids and sulphates allowing them to act as organic ligands for both dissolved and labile particulate fractions within sea ice (Krembs et al.,

2002; Lannuzel et al., 2015). Trace metals can bind to these ligands, increasing the dissolved concentrations, and bind to brine channels walls (Lannuzel et al., 2007, 2015). Phytoplankton were not observed in this ice sample, but they may have been present in the brine allowing for some of the dissolved metals to bind to the channel walls before collection. Regardless of the sorption properties of brine channel walls, the decreasing trend for the trace metals indicates that the release of liquid brine can drive trace metal concentrations in the mixed and columnar ice structures.

Chemical Transformation of Trace Metals in Sea Ice

The concentrations of trace metal size fractions were variable within sea ice. For example, high concentrations of LPFe, DMn and DCd were observed in the granular ice structure (Fig. 6). The presence of high LPFe in granular ice indicated that suspended particles, possibly from sediments, was a major source of LPFe. During turbulent conditions Fe(III) and Fe(II) are released into the overlying water column as sediments are re-suspended (Lohan and Bruland, 2008). Once in the oxic environment Fe(II) is quickly oxidized (Landing and Bruland, 1987) creating particulate Fe oxides. This reaction was estimated to occur within hours in the bottom waters of the Bering Sea (Lohan and Bruland, 2008). As water temperatures cool (-1.86˚C) and turbulent conditions persist, this newly available pool of Fe oxides along with re-suspended sediments containing Fe can accumulate as a result of suspension freezing by frazil ice (Ito et al., 2017).

Granular ice also showed high concentrations of DFe and low concentrations of LPMn (Fig. 6b,c,d). As discussed above, particle entrainment allowed for the accumulation of LPFe

492 into granular ice. Due to their similar behaviors, LPMn concentrations should mimic LPFe, but
493 LPMn concentrations were observed to be low (Fig. 6d). Therefore, the resulting high DMn
494 observed in granular ice can be explained by chemical transformation. The concentration of
495 oxygen in sea ice is low, where brine is supersaturated in oxygen (Glud et al., 2002; Rysgaard
496 and Glud, 2004). Oxygen concentrations in sea ice can further decrease due to organic matter
497 decomposition from bacteria (Rysgaard et al., 2008) or from limited access to wind generated
498 waves (Ackley and Sullivan, 1994; Huang et al., 2017). The nutrient concentrations within the
499 sea ice sample were low (<DL), therefore, brine release had a greater influence on the oxygen
500 concentration. As sediments are re-suspended during turbulent conditions, both Fe and Mn
501 oxides are released into the water column. The oxides are then entrained into frazil ice through
502 suspension freezing. Manganese has a higher reduction potential than Fe (Froelich et al., 1979;
503 Hatta et al., 2013) allowing elevated concentrations of DMn to be represented in the ice
504 structure. Sea ice and snow also have the potential to allow for the photochemical
505 transformation of Mn (LPMn to Mn^{2+}) within its matrixes (Granskog and Kaartokallio, 2004).
506 Another indication for the chemical transformation to dissolved metals in sea ice is its effect on
507 DCd concentrations in granular ice (Fig. 6e,f). At the sediment-water column interface and in
508 surface sediments, Cd is adsorbed onto the surfaces of Fe and Mn oxides. Therefore, the
509 increase in DCd concentrations observed in this sea ice sample is mainly due to release from Fe
510 and Mn oxides during the reduction process (Yu et al., 2000; Huang et al., 2017). This process
511 may also occur in the suboixc areas of sea ice, making chemical transformations another
512 mechanism that can control the concentrations of DMn and DCd.

513 *Summary*

514 In the Arctic Ocean, sea ice is an important player in the biogeochemical cycling of trace
515 metals. However, the processes by which trace metals accumulate into sea ice are not well
516 known. Comparing sea ice structure to trace metal concentrations gives a clearer
517 understanding of these processes. To determine the structure of sea ice, photographic images,
518 porosity % and $\delta^{18}O$ analyses were used. The structures observed in sea ice, from top to
519 bottom, are as follows: snow ice, granular ice, mixed ice and columnar ice. Analysis of the sized
520 fractionated (D, and LP) trace metals (Fe, Mn and Cd) showed that their concentrations differed
521 depending on ice structure. The sea ice used in this study had low salinity indicating a multi-
522 year ice sample. In addition, brine was determined to be released from the sea ice as both
523 nutrients and salinity were observed to be low. Low trace metal concentrations in mixed and
524 columnar ice were also determined to be due to the brine release process. The concentration of
525 Fe, Mn and Cd differed among sea ice structures, indicating that accumulation processes for
526 trace metals are reliant on sea ice formation processes. The observed differences within trace
527 metal size fraction concentrations indicated that there are additional controls through external
528 sources: meteoric snow, particle entrainment, and reductive processes.

529 Figure 7a represents a schematic of the possible accumulation and release processes,
530 and Figure 7b represents the chemical transformation process observed for Mn oxides in
531 granular ice. As Fe and Mn oxides have similar behaviors, Figure 7b will hold true for Fe oxides
532 as well. High concentrations in snow ice indicated that snow ice formation, through the mixing
533 of meteoric snow and seawater, can add atmospheric trace metals. High and heterogeneous
534 concentrations of LPFe in granular ice indicate particle (possible hydroxide and clay particles)
535 entrainment by frazil ice scavenging. During frazil ice formation, sea ice can entrain suspended

536 trace metal bound particles (Fe and Mn) that are reflected in granular ice. Once LPFe and LPMn
537 (oxides) accumulates into sea ice, it can undergo reduction to release DFe, DMn and (adsorbed)
538 DCd in granular ice. This chemical transformation process within sea ice can increase the
539 bioavailability of trace metals. Low trace metal concentrations observed in mixed and columnar
540 ice show that these structures are unable to retain metals following brine drainage. The
541 differences observed in trace metals within sea ice structure show that sea ice formation,
542 chemical reduction, and brine release were the processes behind trace metal accumulation and
543 release in this Arctic sea ice.

544 *Acknowledgments*

545 The authors would like to express our appreciation and thanks to Dr William J. Williams, Dr.
546 Sarah Zimmermann and Dr. Michiyo Yamamoto-Kawai for collecting and providing the Arctic
547 sea ice core. A special thanks to Dr. Michiyo Yamamoto-Kawai for providing the surface
548 seawater $\delta^{18}O$ data. We would like to thank the captain, crew and staff of the *CCGS Louis S. St-*
549 *Laurent* for their assistance and observations during the cruise. We are grateful to Ms. A.
550 Murayama for assistance and support with sample preparations. We would like to thank Dr. T.
551 Toyota for his valuable comments and discussions. We would like to thank D.A. Kelorii for the
552 English editing of this manuscript. We would like to thank the anonymous reviewers for their
553 thoughtful insights that greatly improved our manuscript. Funding was supported by Grant-in-
554 Aid for Scientific Research (A) (No. 17H00775, 17H01157) and Grant-in-Aid for Scientific
555 Research in Innovative Areas (No. JP15H05820) to JN from the Ministry of Education, Culture,
556 Sports, Science and Technology. Research was also supported by the Green Network of
557 Excellence Program (GRENE Program), the Arctic Challenge for Sustainability (ArCS) Project, and

558 partly by the Grant for Joint Research Program of the Institute of Low Temperature Science,
559 Hokkaido University. We are grateful to the Monbukagakusho (MEXT) scholarship for support
560 to LE.

561

562

563 *References*

564 1. Ackley, S.F., Buck, K.R., Taguchi, S., 1979. Standing crop of algae in the sea ice of the
565 Weddell Sea region. Deep-Sea Res. 26A, 269-281.
566 2. Ackley, S.F., Lange, M., Wadhams, P., 1990. Snow cover effects on Antarctic Sea ice
567 thickness. in: Sea ice properties and processes, S. F. Ackley and W. F. Weeks, (Eds),
568 CRREL Monograph 90-1,300 pp.
569 3. Ackley, S.F., Sullivan, C.W., 1994. Physical controls on the development and
570 characteristics of Antarctic sea ice biological communities-a review and synthesis. Deep-
571 Sea Res. I 41, 1583-1604.
572 4. Aguilar-Islas, A.M., Rember, R.D., Mordy, C.W., Wu, J., 2008. Sea ice-derived dissolved
573 iron and its potential influence on the spring algal bloom in the Bering Sea. Geophys.
574 Res. Lett. 35, L24601, https://doi.org/10.1029/2008GL035736.
575 5. Barrie, L.A., 1986. Arctic air pollution: An overview of current knowledge. Atmos.
576 Environ. (1967) 20, 643-663, https://doi.org/10.1016/0004-6981(86)90180-0.
577 6. Bruland, K.W., Lohan, M.C., 2006. Controls of trace metals in seawater. In: Elderfield, H.,
578 Holland, H.D., Turekian, K.K., (Eds.), The Oceans and Marine Geochemistry: Treatise on
579 Geochemistry, Elsevier Ltd., Oxford, pp. 23-47.
580 7. Bruland, K.W., Orians, K.J., Cowen, J.P., 1994. Reactive trace metals in the stratified
581 central North Pacific. Geochim. Cosmochim. Acta 58, 3171-3182.
582 8. Campbell, N.J., Collin, A.E., 1958. The discoloration of Foxe Basin ice. J. Fish. Res. Board
583 Can. 15, 1175-1188.
584 9. Comiso, J. C., Meier, W.N., Gersten, R., 2017. Variability and trends in the Arctic Sea ice
585 cover: Results from different techniques. J. Geophys. Res. Oceans 122, 6883–6900,
586 https://doi.org/10.1002/2017JC012768.
587 10. Cox, G.F.N., Weeks, W.F., 1974. Salinity variations in sea ice. J. Glaciol. 13, 109–120.
588 11. Cox, G.F.N, Weeks. W.F., 1988. Numerical simulations of the profile properties of
589 undeformed first-year sea ice during the growth season. J. Geophys. Res. 93, 12,449–
590 12,460.

12. Darby, D.A., 2003. Sources of sediment found in sea ice from the western Arctic Ocean, new insights into processes of entrainment and drift patterns. J. Geophys. Res. 108, No. C8, 3257, https://doi.org/10.1029/2002JC001350.
13. Dethleff, D., 2005. Entrainment and export of Laptev Sea ice sediments, Siberian Arctic. J. Geophys. Res. 110, https://doi.org/10.1029/2004JC002740.
14. Dethleff, D., Loewe, P., Kleine, E., 1998. The Laptev Sea flaw lead-detailed investigation on ice formation and export during 1991/92 winter season. Cold Reg. Sci. Technol. 27, 225-243.
15. Eicken, H., 2003. From the Microscopic, to the Macroscopic, to the Regional Scale: Growth, Microstructure and Properties of Sea Ice, in: Thomas, D.N., Dieckmann, G.S. (Eds.), Sea Ice: An Introduction to its Physics, Chemistry, Biology and Geology. Blackwell Science Ltd., Oxford, pp. 22-81.
16. Eicken, H., Gradinger, R., Gaylord, A., Mahoney, A., Rigor, I., Melling, H., 2005. Sediment transport by sea ice in the Chukchi and Beaufort Seas: Increasing importance due to changing ice conditions? Deep-Sea Res. II 52, 3281-3302.
17. Eicken, H., Lange, M.L., 1989. Development and Properties of Sea Ice in the Coastal Regime of the Southeastern Weddell Sea. J. Geophys. Res. 94, 8193-8206.
18. Eicken, H., Lensu, M., Lepparanta, M., Tucker, III W.B., Gow, A.J., Salmela, O., 1995. Thickness, structure, and properties of level summer multiyear ice in the Eurasian sector of the Arctic Ocean. J. Geophys. Res. 100, 22,697-22,710.
19. Evans, L., Nishioka, J., 2018. Quantitative analysis of Fe, Mn and Cd from sea ice and seawater in the Chukchi Sea, Arctic Ocean. Polar Sci. 17, 50-58.
20. Fritsen, C. H., Ackley, S. F., Kremer, J. N., Sullivan, C. W., 1998. Flood-Freeze Cycles and Microalgal Dynamics in Antarctic Pack Ice, in: Lizotte, M. P., Arrigo, K. R. (Eds.), Antarctic Sea Ice: Biological Processes, Interactions and Variability. American Geophysical Union, Washington, D. C. https://doi.org/10.1029/AR073p0001.
21. Froelich, P.N., Klinkhammer, G.P., Bender, M.L., Luedtke, N.A., Heath, G.R., Cullen D., Dauphin P., Hammond, D., Harman, B., Maynard, V., 1979. Early oxidation of organic matter in pelagic sediments of the eastern equatorial Atlantic: suboxic diagenesis. Geochim. Cosmochim. Acta 43, 1075-1090.
22. Garrison, D.L., Ackley, S.F., Buck, K.R., 1983. A physical mechanism for establishing algal populations in frazil ice. Nature 206, 363-365.
23. Glud, R.N., Rysgaard, S., Kuhl, M., 2002. A laboratory study on O_2 dynamics and photosynthesis in ice algal communities: Quantification by microsensors, O_2 exchange rates, ^{14}C incubations and PAM fluorometer. Aquat. Microb. Ecol. 27, 301-311.
24. Golden, K.M., Ackley, S.F., Lytle, V.I., 1998. The Percolation Phase Transition in Sea Ice. Science 282, 2238-2241.
25. Granskog, M.A., Kaartokallio, H., 2004. An estimation of the potential fluxes on nitrogen, phosphorus, cadmium and lead from sea ice and snow in the northern Baltic Sea. Water. Air. Soil. Pollut. 154, 331-347.
26. Grotti, M., Soggia, F., Ianni, C., Frache, R., 2005. Trace metals distributions in coastal sea ice of Terra Nova Bay, Ross Sea, Antarctica. Antarc. Sci. 17, 289-300.

27. Guo, T., DeLaune, R.D., Patrick, W.H. Jr., 1997. The influence of sediment redox chemistry on chemically active forms of arsenic, cadmium, chromium and zinc in estuarine sediment. Environ. Int. 23, 305-316.
28. Hatta, M., Measures, C.I., Selph, K.E., Zhou, M., Hiscock, W.T., 2013. Iron fluxes from the shelf regions near the South Shetland Islands in the Drake Passage during the austral - winter 2006. Deep - Sea Res. II 90, 89-101.
29. Hölemann, J.A., Schirmacher, M., Prange, A., 1997. Dissolved and Particulate Major and Trace Elements in Newly Formed Ice from the Laptev Sea (Transdrift III, October 1995), in: Kassens, H., Bauch, H.A., Dmitrenko, I., Eicken, H., Hubberten, H.W., Melles, M., Thiede, J., Timokhov L. (Eds.), Land-Ocean Systems in the Siberian Arctic. Springer, Berlin, pp. 101-111.
30. Hopkins, M. A., Tuhkuri, J., Lensu, M., 1999. Rafting and ridging of thin ice sheets. J. Geophys. Res. 104, 13,605–13,613.
31. Horner, R., Ackley, S.F., Dieckmann, G.S., Gulliksen, B., Hoshiai, T., Legendre, L., Melnikov, I.A., Reeburgh, W.S., Spindler, M., Sullivan, C.W., 1992. Ecology of sea ice biota. Polar Biol. 12, 417-427.
32. Huang, X., Chen, T., Zou, M., Chen, D., Pan, M., 2017. The adsorption of Cd(II) on manganese oxide investigated by batch and modeling techniques. Int. J. Environ. Res. Public Health 14, 1145, https://doi.org/10.3390/ijerph14101145.
33. Hudier, E.J-J., Ingram, R.G., Shirasawa, K., 1995. Upward flushing of sea water through first year ice. Atmos.-Ocean 33, 569-580, https://doi.org/10.1080/07055900.1995.9649545.
34. Ito, M., Ohshima, K.I., Fukamachi, Y., Mizuta, G., Kusumoto, Y., Nishioka, J., 2017. Observations of frazil ice formation and upward sediment transport in the Sea of Okhotsk: A possible mechanism of iron supply to sea ice. J. Geophys. Res.: Oceans 122, 788-802, https://doi.org/10.1002/2016JC012198.
35. Janssens, J., Meiners, K.M., Tison, J-L., Dieckmann, G., Delille, B., Lannuzel, D., 2016. Incorporation of iron and organic matter into young Antarctic sea ice during its initial growth stages. Elementa 4, http://doi.org/10.12952/journal.elementa.000123.
36. Jardon, F.P., Vivieer, F., Vancoppenolle, M., Lourenco, A., Bouruet-Aubertot, P., Cuypers, Y., 2013. Full-depth desalination of warm sea ice. J. Geophys. Res.: Ocean 118, 435-447.
37. Jeroen, O., 2018. magick: Advanced Graphics and Image-Processing in R. R package versi on 1.8. https://CRAN.R-project.org/package=magick.
38. Kempema, E.W., Reimnitz, E., Barns, P.W., 1989. Sea ice sediment entrainment and rafting in the Arctic. J. Sediment. Petrol. 59, 308-317.
39. Kovacs, A., 1996. Sea ice, part I, bulk salinity versus ice floe thickness. CRREL Report 96, 16.
40. Kingery, W.D., Goodnow, W.H., 1963. Brine migration in sea ice, in: Ice and Snow, W.D Kingery (Eds.), M.I.T. Press, pp. 237-247.
41. Krachler, M., Zheng, J., Koerner, R., Zdanowicz, C., Fisher, D., Shotyk, W., 2005. Increasing atmospheric antimony contamination in the northern hemisphere: snow and ice evidence from Devon Island, Arctic Canada. J. Environ. Monit. 12, 1169-1176.

42. Krembs, C., Eicken, H., Junge, K., Deming, J.W., 2002. High concentrations of exopolymer ic substances in Arctic winter sea ice: implications for the polar ocean carbon cycle and c ryoprotection of diatoms. Deep-Sea Res. I 49, 2163-2181.
43. Lampros, Mouselimis, 2018. OpenImageR: An Image Processing Toolkit. R package versi on 1.0.8. https://CRAN.R-project.org/package=OpenImageR.
44. Landing, W.M, Bruland, K., 1987. The contrasting biogeochemistry of iron and manganese in the Pacific Ocean. Geochim. Cosmochim. Acta. 51, 29-43.
45. Lange, M. A., Ackley, S. F., Wadhams, P., Dieckmann, G. S., Eicken, H., 1989. Development of sea ice in the Weddell Sea. Ann. Glaciol. 12, 92–96.
46. Lange, M. A., Eicken, H., 1991. Textural characteristics of sea ice and the major mechanism of ice growth in the Weddell Sea. Ann. Glaciol. 15, 210–215.
47. Lange, M. A., Schlosser, P., Ackley, S.F., Wadhams, P., Dieckmann, G.S., 1990. ^{18}O concentrations in sea ice of the Weddell Sea, Antarctica. J. Glaciol. 36, 315-323, https://doi.org/10.3189/002214390793701291.
48. Lannuzel D., Grotti M., Abelmoschi M.L., van der Merwe P., 2015. Organic ligands control the concentrations of dissolved iron in Antarctic sea ice. Mar. Chem. 174, 120-130.
49. Lannuzel, D., Schoemann, V., de Jong, J., Chou, L., Delille, B., Becquevort, S., Tison, J-L., 2008. Iron study during a time series in the western Weddell pack ice. Mar. Chem. 108, 85-95.
50. Lannuzel, D., Schoemann, V., de Jong, J., Pasquer, B., van der Merwe, P., Masson, F., Tison, J-L., Bowie, A., 2010. Distribution of dissolved iron in Antarctic sea ice: Spatial, seasonal, and inter-annual variability. J. Geophys. Res. 115, G03022 https://doi.org/10.1029/2009JG001031.
51. Lannuzel, D., Schoemann, V., de Jong, J., Tison, J-L., Chou, L., 2007. Distribution and biogeochemical behavior of iron in the East Antarctic sea ice. Mar. Chem. 106, 18-32.
52. Lannuzel, D., Vancoppenolle, M., van der Merwe, P., de Jong, J., Meiners, K.M., Grotti, M., Nishioka, J., Schoemann, V., 2017. Iron in sea ice: Review and new insights. Elementa 4, 000130, https://doi.org/10.12952/journal.elementa.000130.
53. Lohan, M.C., Bruland, K.W., 2008. Elevated Fe(II) and dissolved Fe in hypoxic shelf waters off Oregon and Washington: an enhanced source of iron to coastal upwelling regimes. Environ. Sci. Technol. 42, 6462-6468.
54. Marsay, C.M., Aguilar-Islas, A., Fitzsimmons, J.N., Hatta, M., Jensen, L.T., John, S.G., Kadko, D., Landing, W.M., Lanning, N.T., Morton, P.L., Pasqualini, A., Rauschenberg, S., Sherrell, R.M., Shiller, A.M., Twining, B.S., Whitmore, L.M., Zhang, R., Buck, C.S., 2018. Dissolved and particulate trace elements in late summer Arctic melt ponds. Mar. Chem. 204, 70-85.
55. Maykut, G.A., 1985. The ice environment, in: Horner, R.A. (Eds.) Sea Ice Biota. CRC Press Inc., Florida, pp. 21-82.
56. Minami, T., Konagaya, W., Zheng, L., Takano, S., Sasaki, M., Murata, R., Nakaguchi, Y., Sohrin, Y., 2015. An off-line autHopkinsomated preconcentration system with ethylenediaminetriacetate chelating resin for the determination of trace metals in seawater by high-resolution inductively coupled plasma mass spectrometry. Anal. Chim. Acta 854, 183-190.

57. Nishioka, J., Takeda, S., Wong, C.S., Johnson, W.K., 2001. Size-fractionated iron concentrations in the northeast Pacific Ocean: Distribution of soluble and small colloidal iron. Mar. Chem. 74, 157-179.
58. Nürnberg, D., Wollenburg, I., Dethleff, D., Eicken, H., Kassens, H., Letzig, T., Reimnitz, E., Thiede, J., 1994. Sediments in Arctic sea ice: Implications for entrainment, transport and release. Mar. Geol. 119, 185-214.
59. Osterkamp, T.E., Gosink, J.P., 1984. Observations and analyses of sediment-laden sea ice, in: Barnes, P.W., Schell, D.M., Reimnitz, E., (Eds.), The Alaskan Beaufort Sea: Ecosystems and environments, Academic Press, University of California pp. 73-93.
60. Overland, J.E., Hanna, E., Hanssen-Bauer, I., Kim, S-J., Walsh, J.E., Wang, M., Bhatt, U.S., Thoman, R.L., 2017. Surface Air Temperature [in Arctic Report Card 2017], http://ww.arctic.noaa.gov/Report-Card.
61. Pardue, J.H., DeLaune, R.D., Patrick, W.H. Jr., 1992. Metal to Aluminum Correlation in Louisiana Coastal Wetlands: Identification of Elevated Metal Concentrations. J. Environ. Qual. 21, 539-545.
62. Perovich, D., Meier, W., Tschudi, M., Farrell, S., Hendricks, S., Gerland, S., Hass, C., Krumpen, T., Polashenski, C., Ricker, R., Webster, M., 2017. Sea Ice [in Arctic Report Card 2017], http://ww.arctic.noaa.gov/Report-Card.
63. Petrich, C., Eicken, H., 2010. Growth, Structure and Properties of Sea Ice. in: Thomas, D.N., Dieckmann, G.S. (Eds.) Sea Ice. 2nd ed. Blackwell Publishing Ltd., Oxford, pp. 23-77.
64. Planchon, F.A.M., Gabrielli, P., Gauchard, P.A., Dommergue, A., Barbante, C., Cairns, W.R.L., Cozzi, G., Nagorski, S.A., Ferrari, C.P., Boutron, C.F., Capodaglio, G., Cescon, P., Varga, A., Wolff, E.W., 2004. Direct determination of mercury at the sub-picogram per gram level in polar snow and ice by ICP-SFMS. J. Anal. At. Spectrom. 19, 823-830, https://doi.org/10.1039/b402711f
65. Przybylak, R., 2007. Recent air-temperature changes in the Arctic. Ann. Glaciol. 46, 316-324.
66. R Core Team (2013). R: A language and environment for statistical computing. R Foundation for statistical Computing, Vienna, Austria. URL http://www.R-project.org/.
67. Reimnitz, E., Dethleff, D., Nürnberg, D., 1994. Contrasts in Arctic shelf sea-ice regimes and some implications: Beaufort Sea versus Laptev Sea. Mar. Geol. 119, 215-225.
68. Reimnitz, E., Marincovich, Jr L., McCormick, M., Briggs, W.M., 1992. Suspension freezing of bottom sediment and biota in the Northwest Passage and implications for Arctic Ocean sedimentation. Can. J. Earth Sci. 29, 693-703.
69. Rysgaard, S., Glud, R.N., 2004. Anaerobic N_2 production in Arctic sea ice. Limnol. Oceanogr. 49, 86-94.
70. Rysgaard, S., Glud, R.N., Sejr, M.K., Blicher, M.E., Stahl, H.J., 2008. Denitrification Activity and oxygen dynamics in Arctic Sea Ice. Polar Biol. 31, 527-537, https://doi.org/10.1007/s00300-007-0384-x.
71. Saager, P.M., de Baar, H.J.W., Burkill, P.H. 1989. Manganese and iron in Indian Ocean waters. Geochim. Cosmochim. Acta 53, 2259 – 2267.
72. Sedwick, P.N., DiTullio, G.R., 1997. Regulation of algal blooms in Antarctic shelf waters by the release of iron form melting sea ice. Geophys. Res. Lett. 24, 2515-2518.

73. Sohrin, Y., Bruland, K.W., 2011. Global status of trace elements in the ocean. Trends Analyt. Chem. 30, 1291-1307.
74. Spindler, M., 1994. Notes on the biology of sea ice in the Arctic and Antarctic. Polar Biol. 14, 319-324.
75. Squire, V.A., Moore, S.C., 1980. Direct measurement of the attenuation of ocean waves by pack ice. Nature 283, 365-368.
76. Takeda, S., Obata, H., 1995. Response of equatorial Pacific phytoplankton to subnanomolar Fe enrichment. Mar. Chem. 50, 219-227.
77. Thomas, D.N., Papadimitriou, S., Michel, C., 2010. Biogeochemistry of Sea Ice, in: Thomas, D.N., Dieckmann, G.S. (Eds.), Sea Ice 2nd ed. Blackwell Publishing Ltd., Oxford, pp. 425-455.
78. Tovar-Sanchez, A., Duarte, C.M., Alonso, J.C., Lacorte, S., Tauler, R., Galban-Malagon, C., 2010. Impacts of metals and nutrients released from melting multiyear Arctic sea ice. J. Geophys. Res. 115, C07003 https://doi.org/10.1029/2009JC005685.
79. Toyota, T., Kawamura, T., Ohshima, K.I., Shimoda, H., Wakatsuchi, M., 2004. Thickness distribution, texture and stratigraphy, and a simple probabilistic model for dynamical thickening of sea ice in the southern Sea of Okhotsk. J. Geophys. Res. 109, C06001, https://doi.org/10.1029/2003JC002090.
80. Toyota, T., Takatsuji, S., Tateyama, K., Naoki, K., Ohshima, K.I., 2007. Properties of sea ice and overlying snow in the southern Sea of Okhotsk. J. Oceanogr. 63, 393-411.
81. Ukita, J., Kawamura, T., Tanaka, N., Toyota, T., Wakatsuchi, M., 2000. Physical and stable isotopic properties and growth processes of sea ice collected in the southern Sea of Okhotsk. J. Geophys. Res. 105, 22,083–22,093.
82. Untersteiner, N., 1968. Natural desalination and equilibrium salinity profile of perennial sea ice. J. Geophys. Res. 73, 1,251-1,257.
83. van der Merwe, P.C., Lannuzel, D., Bowie, A.R, Mancuso Nichols, C.A., Meiners, K.M., 2011. Iron fractionation in pack and fast ice in East Antarctica: Temporal decoupling between the release of dissolved and particulate iron during spring melt. Deep-Sea Res. II 58, 1222-1236.
84. Weeks, W.F., Ackley, S.F., 1986. The growth, structure and properties of sea ice, in: Untersteiner, N. (Eds.), The Geophysics of Sea Ice. Plenum Press, New York, pp 9-164.
85. Weingartner, T. J., Cavalieri, D.J., Aagaard, K., Sasaki, Y., 1998. Circulation, dense water formation, and outflow on the northeast Chukchi Shelf. J. Geophys. Res., 103, 7647–7661, https://doi.org.10.1029/98JC00374.
86. Weissenberger, J., Dieckmann, G., Gradinger, R., Spindler, M., 1992. Sea ice: A cast technique to examine and analyze brine pockets and channel structure. Limnol. Oceangr. 37, 179-183.
87. Weissenberger, J., Grossmann, S., 1998. Experimental formation of sea ice: importance of water circulation and wave action for incorporation of phytoplankton and bacteria. Polar Biol. 20, 178-188.
88. Yamamoto-Kawai, M., McLaughlin, F.A., Carmack, E.C., Nishino, S., Shimada, K., 2008. Freshwater budget of the Canada Basin, Arctic Ocean, from salinity, $\delta^{18}O$, and Nutrients. J. Geophys. Res. 113, C01007, https://doi.org/10.1029/2006JC003858.

89. Yu, K-T., Lam, M.H-W., Yen, Y-F., Leung, A.P.K., 2000. Behavior of trace metals in the sediment pore waters of intertidal mudflats of a tropical wetland. Environ. Toxicol. Chem. 19, 535-542.

Figure Captions

Figure 1. Picture and schematic of cold tub used during the ice core planing step. Cold tub was cooled to -20˚C by cooling coils located inside the tub's chamber. The temperature inside the chamber remained consistent below a temperature limit line. Above this line the temperatures significantly increased. a) Picture of cold tub, b) cooling coils, c) pre-set temperature limit line, and d) ice planing step.

Figure 2. Location of sea ice sampling site. Sea ice concentration on August 24, 2013 (24 hr average) from ECMWF metadata. Black dot - Location of the ice station where sea ice was collected.

Figure 3. Photo and schematic of ice core structure. a) Photo of ice core taken after collection from coring with the depth representing the length of the core, b) photos taken after planing (2 cm), c) transformed planed photo to black and white, with a filter overlaid, to represent the outline of the micropores (porosity %), d) schematic of observed sea ice structure. 0 - 24 cm snow ice, 24 - 75 cm granular ice, 75 - 91 cm mixed ice and 91 - 103 cm columnar ice.

Figure 4. Milli-Q Ice Contamination Test. Concentrations of a) Fe, b) Mn, and c) Cd in Milli-Q ice without foil (Milli-Q Clean Ice) and Milli-Q ice wrapped in aluminum foil (Foil Ice). Samples were planed up to 2 cm and each layer (Layer 1 – Outer 1 cm of ice, Layer 2 – Inner 1 cm of Ice, Core – Cleaned ice) was pre-concentrated with the NOBIAS resin. Presented values were above the pre-concentrated DL and then calculated with the pre-concentration factor (4.5 - 8.6 times). The pre-concentration factor was determined by the sample weights before pre-concentration and the eluent weights after pre-concentration.

Figure 5. Salinity and $\delta^{18}O$ for each ice structure. a) Salinity, b) $\delta^{18}O$, dotted line represents $\delta^{18}O$ values from the surrounding surface seawater (<50 m; Yamamoto-Kawaii personal comm.).

Figure 6. Concentrations of dissolved and labile particulate metals for snow ice, granular ice, mixed ice and columnar ice. The ice core depth is represented on the y-axis. Error bars are SD from GFAAS measurement data. a) DFe, b) LPFe, c) DMn, d) LPMn, e) DCd, f) LPCd.

Figure 7. a) Schematic of trace metal accumulation and release processes in multi-year Arctic sea ice, and b) schematic of chemical reduction process for multi-year Arctic sea ice.

a)

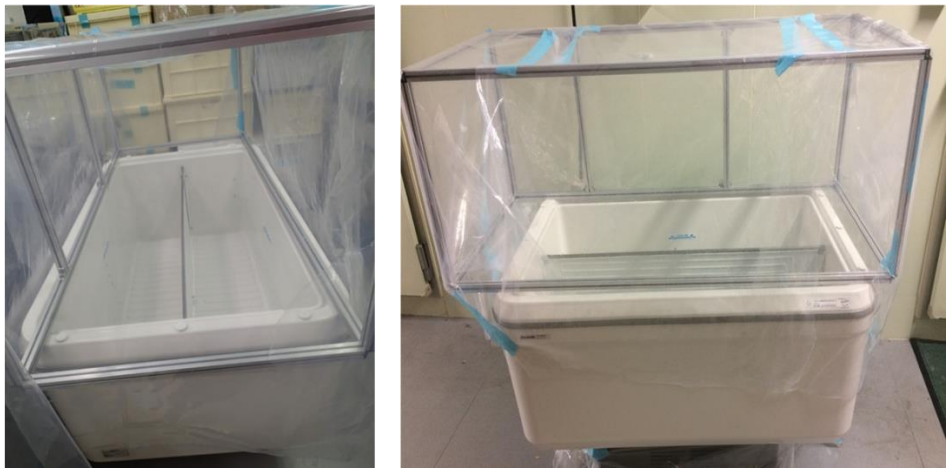

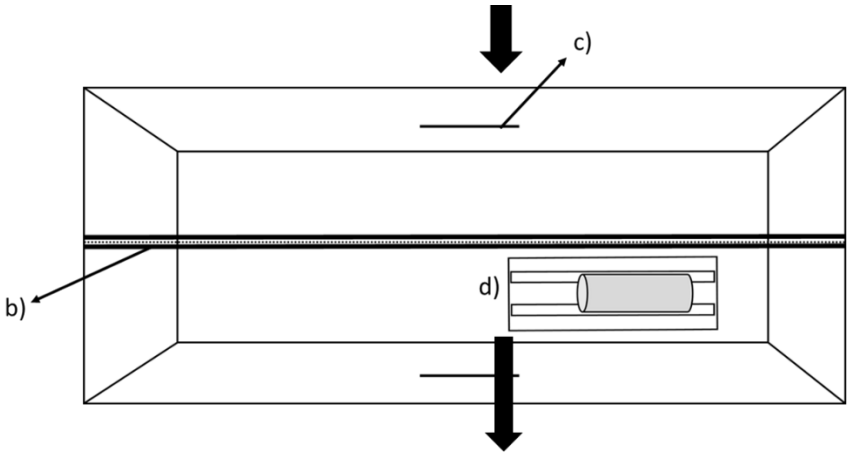

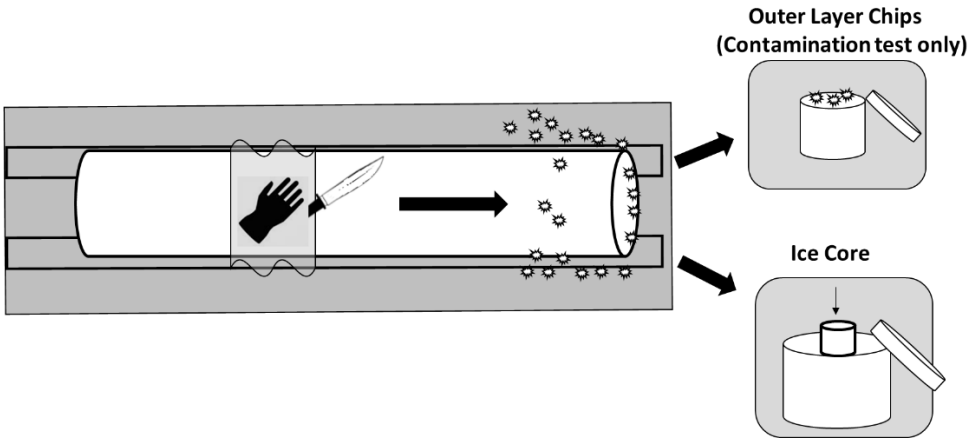

Figure 1

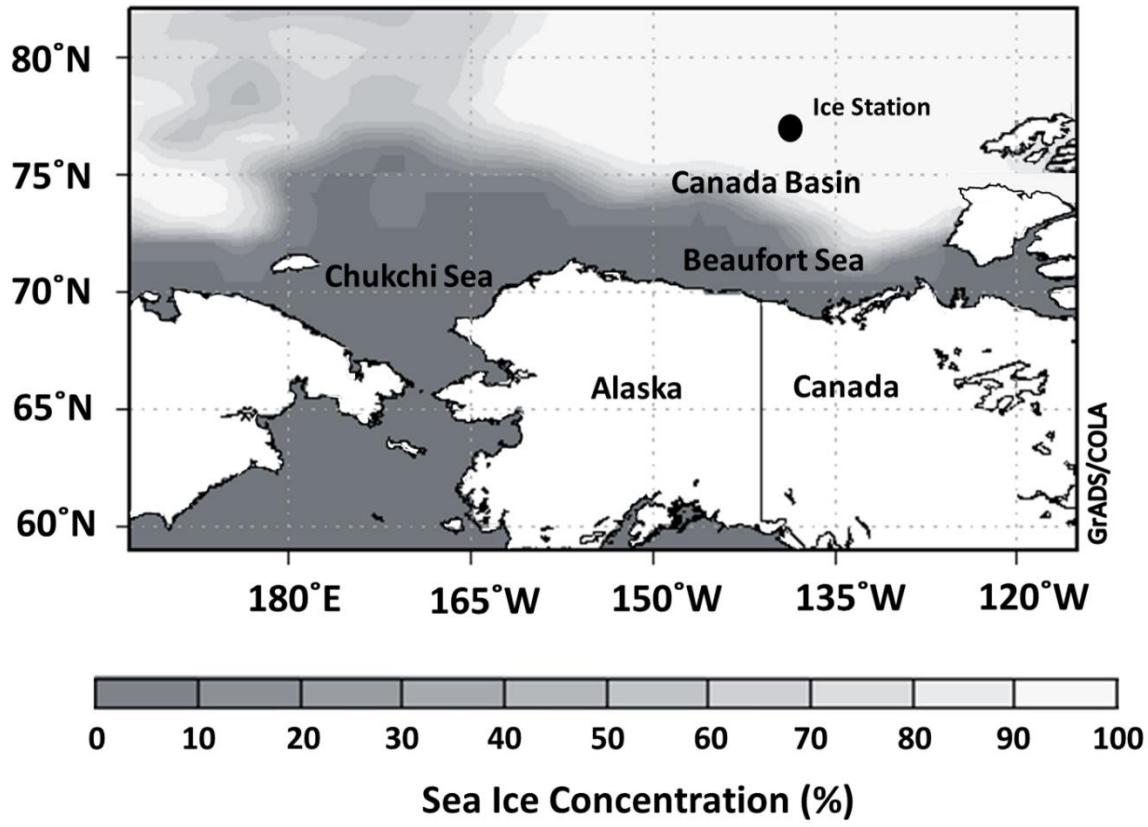

842

843 Figure 2

844

845

846

847

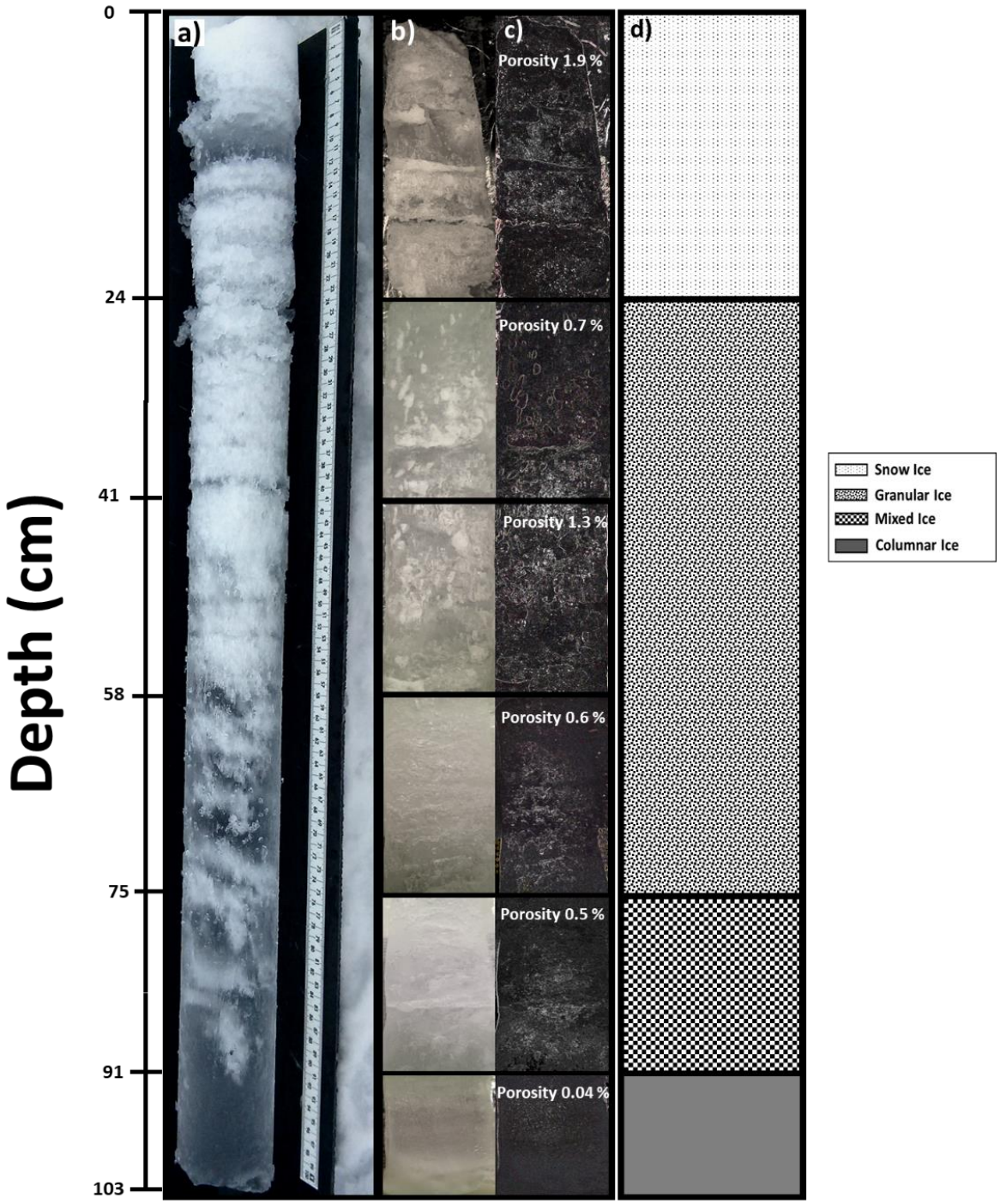

848

849 Figure 3

850

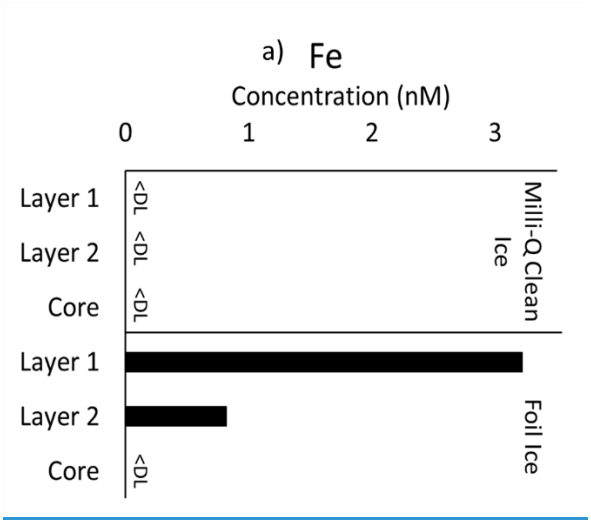

851

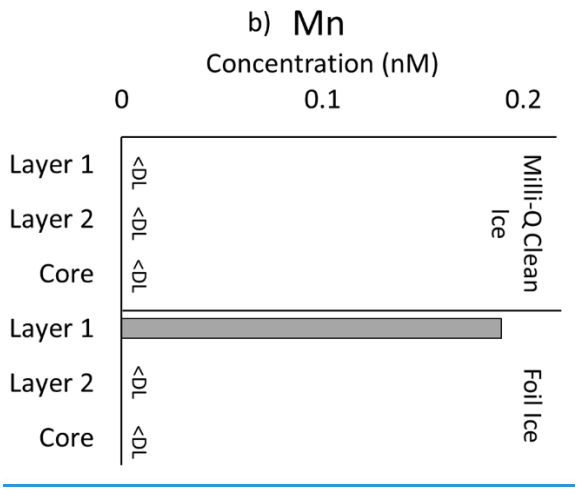

852

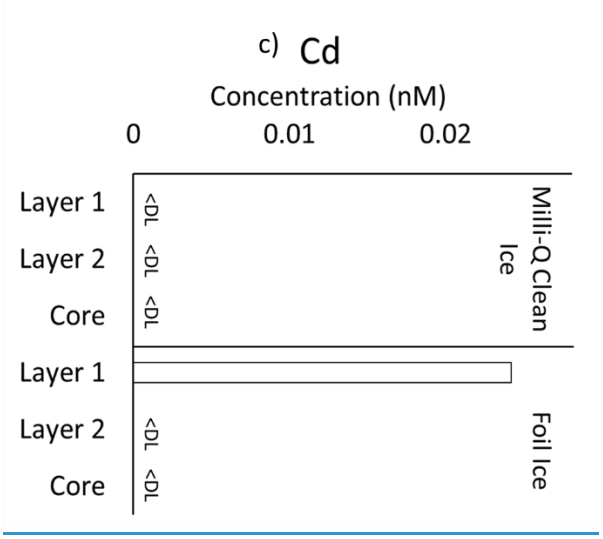

853

854 Figure 4.

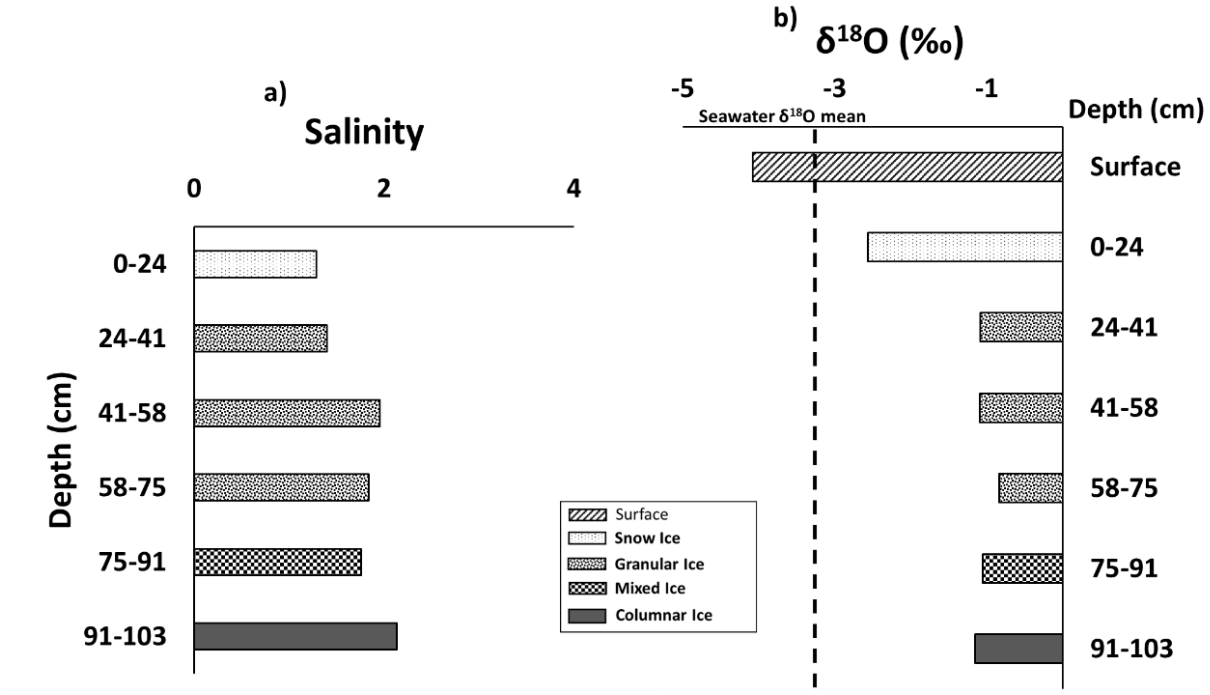
a)
Salinity
0
2
4
Depth (cm)
0-24
24-41
41-58
58-75
75-91
91-103
Surface
Snow Ice
Granular Ice
Mixed Ice
Columnar Ice
b)
δ18O (‰)
-5
-3
-1
Seawater δ18O mean
Depth (cm)
Surface
0-24
24-41
41-58
58-75
75-91
91-103

Figure 5.

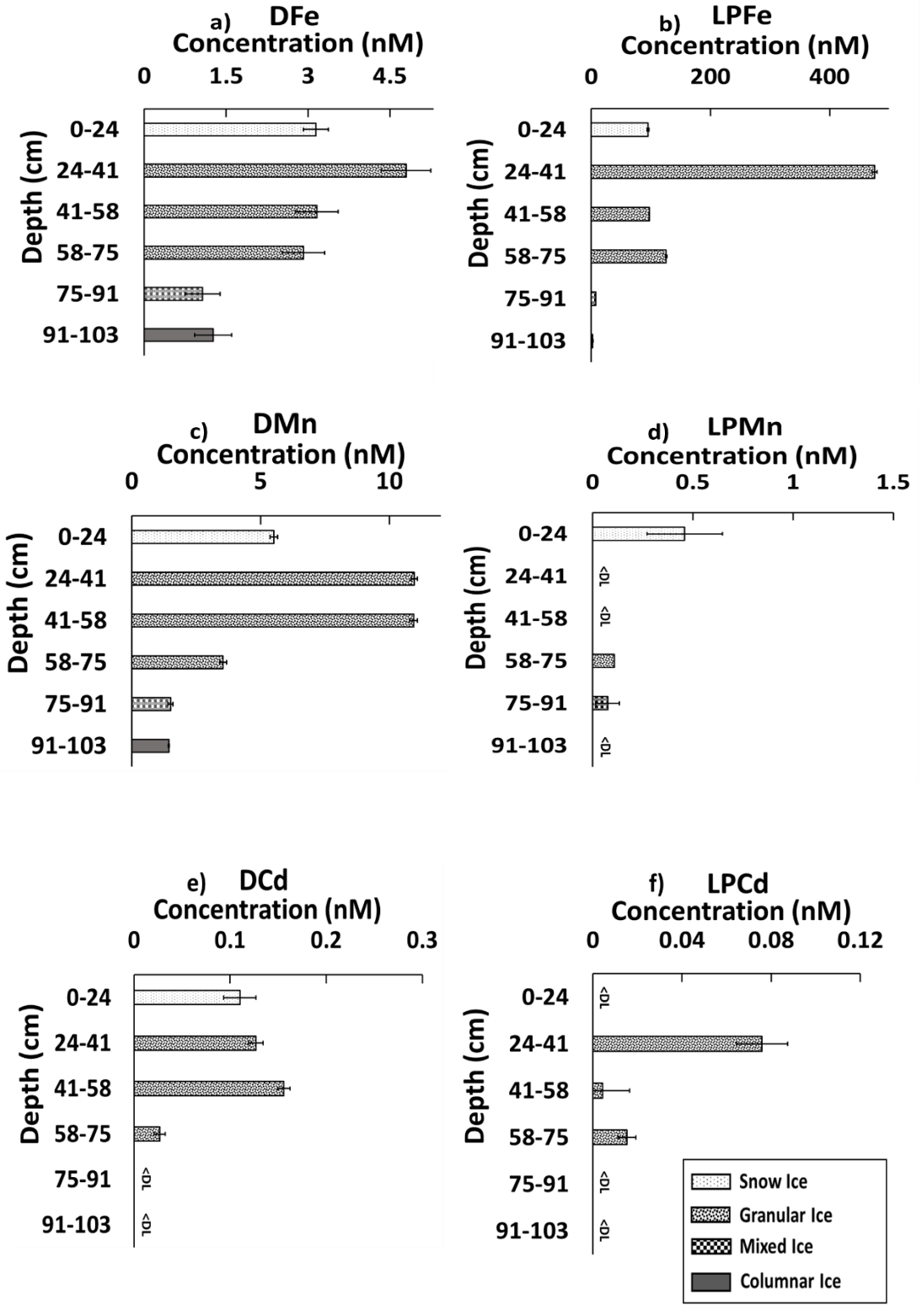
a) DFe
Concentration (nM)
0
1.5
3
4.5
Depth (cm)
0-24
24-41
41-58
58-75
75-91
91-103
b) LPFe
Concentration (nM)
0
200
400
c) DMn
Concentration (nM)
0
5
10
d) LPMn
Concentration (nM)
0
0.5
1
1.5
BDL
e) DCd
Concentration (nM)
0
0.1
0.2
0.3
f) LPCd
Concentration (nM)
0
0.04
0.08
0.12
Snow Ice
Granular Ice
Mixed Ice
Columnar Ice

Figure 6

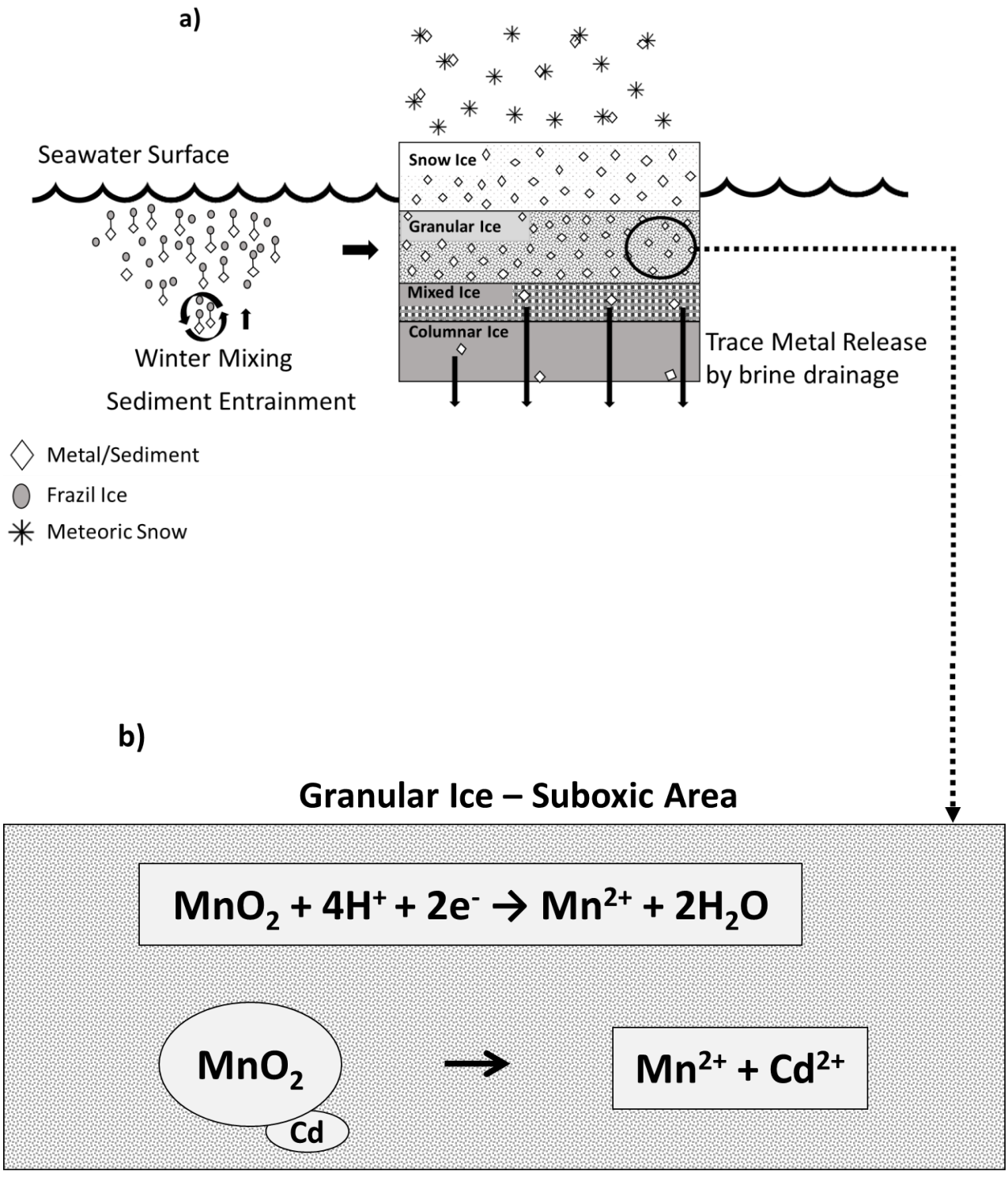

865

866

867 Figure 7

868